NAMT
95-009

The Hysteric Event in the Computation of Magentization

David Kinderlehrer
Ling Ma
Carnegie Mellon University

Research Report No. 95-NA-009

April 1995

Sponsors

U.S. Army Research Office
Research Triangle Park
NC 27709

National Science Foundation
1800 G Street, N.W.
Washington, DC 20550

The hysteretic event in the computation of magnetization

David Kinderlehrer and Ling Ma

Department of Mathematics and Center for Nonlinear Analysis
Carnegie Mellon University
Pittsburgh, PA. 15213-3890

1. Introduction Simulations of magnetic and magnetostrictive behavior based on micromagnetic theory exhibit hysteresis. These systems have a highly nonlinear character involving both short range anisotropy and elastic fields and dispersive demagnetization fields. Hysteresis occurs even in the absence of an imposed dynamical mechanism, for example, a Landau-Lifshitz-Gilbert dissipative equation for the magnetic moment, and is symptomatic of the way the system navigates a path through local minima of its energy space. It is not sensitive to the particular method: we implement continuation based on the conjugate gradient method, although the same results were obtained by other methods (eg., Newton's) as well. We strive to attain an efficient algorithm with careful attention dedicated to the treatment of the demagnetization energy. It is robust: computational experiments confirm that the shape of the loop is invariant over several decades of mesh refinement. Nonetheless, the propensity of optimization procedures to become marooned at local extrema when applied to nonconvex situations presents a fundamental challenge to analysis. Understanding and controlling such phenomena present the opportunity to develop predictive tools and diagnostics[1].

Computational results and diagnostics, developed using contemporary nonlinear analysis, are presented. As illustrations: Since the energy picture is mesh independent, computing on a fairly coarse grid suffices to establish its character. In simple cases, the precise destabilization effect of

[1] Supported by AFOSR 91 0301 and NSF DMS 911572 and by the ARO and the NSF through the Center for Nonlinear Analysis at Carnegie Mellon University. Computational resources provided by the NSF through a grant to the Pittsburgh Supercomputing Center.

the induced magnetic field together with the width of the hysteresis loop may be determined analytically in terms of a correction to the Stoner-Wohlfarth Theory [44].

The computation of microstructure based on continuum theory is one area where these problems have been discussed [7,8,9,28,29,31,37]. Recent related thoughts about hysteretic behavior, principally in shape memory or pseudoelastic materials, may be found in [1,2,4,13,14,16,34, 35,38,42,45]. We note in §8 that we have computed hysteresis for models of some of these materials also. A conceptually different approach to the computation of magnetic hysteresis is given by Giles et al. [15], cf. also [3].

A characteristic of the hysteretic cycle is that the system does not always assume a minimum energy state. Theories and models of hysteresis (cf. [32,33,46] for compendia of these), pose rules to describe the paths hysteresis follow, but not why hysteresis occurs. Basics of Preisach modeling, for example, are given there and in Mayergoyz [33] and Wiesen and Charap [47]. This type of phenomenological modeling is very useful in complex systems. It may accomodate domain wall motion and active constraints whose precise behavior at the microstructural level is extremely complicated.

2. Formulation We consider a two dimensional system governed by a magnetic anisotropy energy $\varphi(m)$ subjected to an external field H. This gives rise to a stored energy to which we add the energy of the induced magnetic field, usually referred to as the demagnetization energy, resulting in the functional

$$E(H,m) = \int_{\Omega} (\varphi(m) - H\cdot m)\, dx + \frac{1}{2} \int_{\mathbf{R}^2} |\nabla u|^2\, dx, \tag{2.1}$$

with

$$\operatorname{div}(-\nabla u + m\chi_{\Omega}) = 0, \quad |m| = 1 \text{ in } \Omega.$$

The second equation embodies Maxwell's equations for magnetostatics. The constraint on the magnetization m represents the requirement that the material be magnetically saturated. The domain Ω is the region occupied by the magnet. Equivalently, we may write

$$E(H,m) = \int_{\Omega} (\varphi(m) - H\cdot m)\, dx + \frac{1}{2} \int_{\Omega} \nabla u\cdot m\, dx, \tag{2.1'}$$

Typical forms for φ are

$$\varphi(m) = \kappa (m_2)^2 \qquad \text{(uniaxial)} \tag{2.2}$$

$$\varphi(m) = \kappa (m_1 m_2)^2 \qquad \text{(cubic)} \tag{2.3}$$

In the uniaxial case, when $\kappa > 0$, e_1 is the easy axis and when $\kappa < 0$, e_2 is the easy axis. In the cubic case, when $\kappa > 0$, e_1 and e_2 are easy axes and when $\kappa < 0$, $e_1 \pm e_2$ are easy axes. In our simulations we chose $\Omega = (0,L) \times (0,1)$, a rectangle.

Our computational technique applies equally well to linear magnetostriction, cf. Clark [6]. A major reason for studying both rigid magnets and linear elastic ones is to gain experience useful to analyze highly magnetostrictive materials, cf. [10,11,12,17,18,19,20,21,22,23,24,25,26,41]. In two dimensional linear magnetostriction, the material is endowed with a stored energy $\varphi(\varepsilon,m)$ which has the form

$$\varphi(\varepsilon,m) = \varphi_{el}(\varepsilon) + \varphi_{el/mag}(\varepsilon,m) + \varphi_{an}(m),$$

$$\varepsilon = \tfrac{1}{2}(\nabla y + \nabla y^T), \quad |m| = 1, \ y \text{ the displacement.}$$

The elastic energy $\varphi_{el}(\varepsilon)$ is a typical linear elastic energy with cubic symmetry or lower. The elastic/magnetic interaction has the form

$$\varphi_{el/mag}(\varepsilon,m) = \sum b_{ij}\, \varepsilon_{ij}\, m_i m_j .$$

Note that it is even in m. The anisotropy energy $\varphi_{an}(m)$ is given by (2.2) or (2.3). The analogue of (2.1) is

$$E(H,y,m) = \int_\Omega (\varphi(\varepsilon,m) - m\cdot H)\, dx + \frac{1}{2} \int_{R^2} |\nabla u|^2\, dx. \qquad (2.3)$$

Recently we have computed (2.3) for magnetostriction, we have not as yet obtained any estimates which include the effects of elasticity [24].

For minimum energy at given H, one seeks

$$\inf_{\{|m| = 1\}} E(H,m) \quad \text{or} \quad \inf_{\{|m| = 1\}} E(H,y,m) \quad \text{subject to boundary conditions.}$$

The presence of a hysteresis curve in the ensuing computation is evidence that minimum energy is not actually achieved. Nonetheless, it remains useful to know the relaxation of the energy E(H,m) or E(H,y,m). We have computed some cases of the latter with Chipot [5] along the lines of argument described in Kohn [27].

3. Description of hysteresis We describe the hysteretic event. The hysteresis diagram for the energy (2.1) is computed by continuation of resolved solutions with respect to decreasing and increasing magnetic field applied parallel to the x_1-axis, which is also the easy axis. The shown curves in Figs 4 and 5 are the overlaid graphs of computed energies vs. a decreasing sequence of applied fields and an increasing sequence of applied fields.

The computational domain is a rectangle $\Omega = (0,L) \times (0,1)$, usually with $L = 2$, and oriented so that the x_1 axis is an easy direction. We partition Ω into $N_1 \times N_2$ squares of side length $h = L/N_1 = 1/N_2$ denoted by

$$\Omega_{ij} = \{x \in \Omega: ih < x_1 < (i+1)h,\ jh < x_2 < (j+1)h\},$$

$i = 0, \ldots, N_1 - 1$, $j = 0,1,\ldots,N_2 - 1$. The minimization of (2.1) is approximated in the space A_h by the Polak-Ribière version of the conjugate gradient method [40,43] where

$$A_h = \{ m: m \text{ is constant on each } \Omega_{ij}, i = 0, \ldots, N_1 - 1,\ j = 0,1,\ldots,N_2 - 1\}.$$

For a given initialization μ, let $T(\mu)$ denote the computed minimizer for the functional (2.1). Let H_o be the maximum external field strength, n be a positive integer, and $\delta = 2H_o/n$. We simulate the hysteresis by this algorithm:

1. Initialize m, set $H = (H_o,0)$, and compute $m^0 = T(m)$.

2. For $k = 1,2,\ldots,n$, set $H^k = (H_o - k\delta,0)$ and compute $m^k = T(m^{k-1})$.

3. For $j = 1,2,\ldots,n$, set $H^j = (-H_o + j\delta,0)$ and compute $m^j = T(m^{j-1})$, with m^0 set to m^n from 2.

The shown diagrams in Figures 4 and 5 are then the overlaid graphs of $(H^k, E(H^k,m^k))$ and $(H^j, E(H^j,m^j))$.

We recall the essential features of this conjugate gradient algorithm. It is an optimization method which resolves the magnetization (and displacements, when elastic effects are included) in all the cells simultaneously. The induced or demagnetizing field is taken as a function of the magnetization. The minimization algorithm requires the computation of energy and also the gradient of the energy with respect to the discrete variables for a given set of $m \in A_h$. We remark that the most expensive feature of these computations is the determination of the averages of ∇u on the cells Ω_{ij}, i.e.,

$$\overline{\nabla u}_{ij} = \frac{1}{h^2} \int_{\Omega_{ij}} \nabla u \, dx.$$

We refer to Luskin and Ma [28,29] for details.

Our implementation is efficient; the subsequence hysteresis loop is computed in about three minutes of CPU time at over 300 MFLOPS of the CRAY YMP-C90 at the Pittsburgh Supercomputing Center.

The configuration begins at an absolute minimum of energy, or nearly so, for a large value of H_o and remains in this state until H^k changes sign. For these values of H^k, $m^k \approx m^0$,

which we refer to as the precursor magnetization. This precursor magnetization is quite close to e_1.

The system then traverses a metastable regime where it does not achieve minimum energy. Some small oscillations are observed in this regime. The metastable regime ends in a critical field range which appears to be characterized by the condition that the precursor magnetization becomes unstable at the critical field, H_{cr},

$$E(H_{cr},m) \leq E(H_{cr},m^0) \quad \text{for appropriate } m.$$

In fact, it seems that the computation seeks to resolve the closure domains, or boundary columns of the computational grid, first. We shall use this as the basis for our estimate of H_{cr}.

Near $H = H_{cr}$, the system suffers instability and witnesses rapid interior oscillations, the evolution of microstructural domain configurations, and finally resolution to a nearly uniform state of approximately absolute minimum energy. The behavior of the system is analogous to the classical Stoner-Wohlfarth scenario [44], which we review below. Müller and Xu [35] also observe a stable/ metastable/ unstable/ stable sequence in the extension of shape memory ribbons. We do not see this behavior when the applied field H is parallel to the hardest axis, which is x_2 in the uniaxial case and $x_1 \pm x_2$ in the cubic case. Indeed, there is almost no hysteresis in the hard axis uniaxial situation.

Here we are discussing only the major loops of the system, which are the overlaid graphs mentioned above. We have also computed minor loops and the virgin magnetization curve. Explicit computation of virgin magnetization curves based on minimum energy, cf. below, have been given by DeSimone.

4. An elementary observation, the Stoner-Wohlfarth theory A glimpse at the Stoner-Wohlfarth theory shows that the general outline of the energy portrait is already present when the demagnetization energy is neglected and the system evolves by exchange of stability among local minima. In their fundamental work, Stoner and Wohlfarth studied the behavior of the homogeneously magnetized ellipsoid, exploiting the property, known to Dirichlet, that if the magnetization is a constant vector parallel to a principle axis of the ellipsoid Ω, then the solution of

$$\Delta u = \operatorname{div} m\chi_\Omega \quad \text{in } \mathbb{R}^3$$

is linear when restricted to Ω. In two dimensions, for example, with B the unit ball, it is easy to check that for u satisfying

$$\Delta u = \operatorname{div} \xi\chi_B \quad \text{in } \mathbb{R}^2, \ \xi \text{ constant, with } \nabla u \in L^2(\mathbb{R}^2),$$

we have that

$$\nabla u = \tfrac{1}{2}\xi \quad \text{in } B \text{ and}$$

$$\frac{1}{2}\int_B \nabla u\cdot\xi\, dx = \frac{1}{2}\int_{R^2} |\nabla u|^2\, dx = \frac{\pi}{4}|\xi|^2 . \qquad (4.1)$$

So if m is constant and $|m| = 1$, the induced field energy in (2.1) is simply a constant. In the basic Stoner-Wohlfarth framework, the system is regarded as homogeneous with energy given by the function

$$E(H,m) = \varphi(m) - m\cdot H + \frac{1}{4} \qquad (4.2)$$

per unit area.

Consider the uniaxial case with easy axis the x_1-axis and choosing $H = (H_1,0)$. Here, E(H,m) has the appearance of a double well potential since it is given by

$$E(H,m) = -\kappa(m_1 + \frac{H_1}{2\kappa})^2 + \text{const.}$$

Following the easy axis starting with large positive H_1, we see that $m = e_1$ is an absolute minimum for $H_1 \geq 0$, it is stable for $-2\kappa \leq H_1 < 0$, and unstable for $H_1 < -2\kappa$. In the region $H_1 \leq 0$, the absolute minimum is attained by $-e_1$. We have drawn in Figure 1 the absolute and relative minimizing energy curves obtained by following a cycle from $(H_o,0)$ to $(-H_o,0)$ and returning to $(H_o,0)$. The critical field is $H_{SW} = 2\kappa$. We refer to this value as the Stoner-Wohlfarth critical field.

Turning to the uniaxial case with hard axis the x_1-axis, E(m,H) will have the appearance of a convex function, indeed, denoting the anisotropy constant by $-\kappa$, with $\kappa > 0$,

$$E(H,m) = \kappa(m_1 - \frac{H_1}{2\kappa})^2 + \text{const.}$$

Following the hard axis, we see that the system remains in a state of absolute minimum given by

$$m = \begin{cases} e_1 & \frac{H_1}{2\kappa} \geq 1 \\ (\frac{H_1}{2\kappa}, \pm\sqrt{1-(\frac{H_1}{2\kappa})^2}) & |\frac{H_1}{2\kappa}| < 1 \\ -e_1 & \frac{H_1}{2\kappa} < -1 \end{cases} .$$

Hence the Stoner-Wohlfarth analysis gives a good cartoon of what we see in the computation.

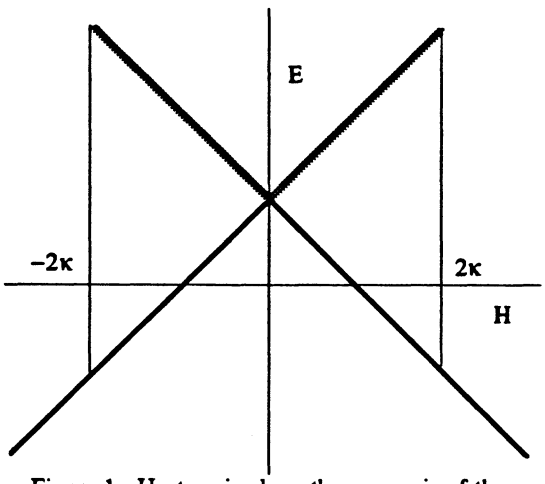

Figure 1. Hysteresis along the easy axis of the Stoner -Wohlfarth system.

The curve of minimum energy is different. It is not even the black Λ of Figure 1. This is because, as described in [10,11,18], fine phase laminates may result in homogeneous macroscopic magnetizations ξ with $|\xi| < 1$. More precisely, we may find a sequence $m^k \in L^\infty(\mathbb{R}^2;S^1)$ with

$$m^k \rightharpoonup \xi = (\xi_1,0) \quad \text{and}$$
$$E(H,m^k\chi_B) \to \tfrac{1}{4}\xi_1^2 - \xi_1 H_1 .$$

The expression for the limit energy on the right is minimized at $\xi_1 = 2H_1$ for $|H_1| < \frac{1}{2}$. DeSimone [10] has shown that the minimum is represented by the average magnetization ξ and results from the minimizing sequence $(m^k\chi_B)$ with

$$m^k(x) = \begin{cases} e_1 & \frac{j}{k} < x_2 < \frac{j}{k} + \frac{\lambda}{k} \\ -e_1 & \frac{j}{k} + \frac{\lambda}{k} < x_2 < \frac{j+1}{k} \end{cases} , \quad -\infty < j < \infty, \text{ and}$$

$$\lambda = \tfrac{1}{2}(2H_1 + 1).$$

We then have for $H = (H_1,0)$

$$E_{min}(H) = \begin{cases} -H_1^2 & |H_1| < \frac{1}{2} \\ -|H_1| + \frac{1}{4} & |H_1| \geq \frac{1}{2} \end{cases} ,$$

as shown for comparison in Figure 2. More generally, there is a relaxed functional which gives the minimum energy of the system, cf. DeSimone [10] and Pedregal [39].

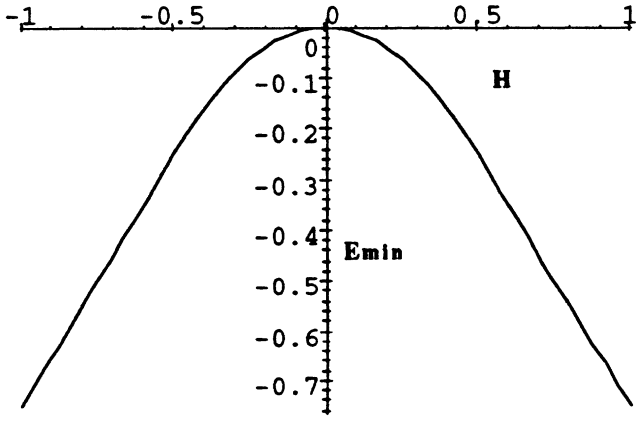

Figure 2. Sketch of minimum energy curve as applied field varies along an easy axis

5. Critical field and width of the hysteresis loop for the easy axis We shall exploit the observation that the computation first seeks to resolve the closure domains, the first and last columns of the computational domain, to estimate the critical field and the width of the hysteresis loop. At this field value, the precursor magnetization $m^0 \approx \pm e_1$ loses stability. The estimate is sought as a domain dependent correction to the Stoner-Wohlfarth critical field value $H_{SW} = 2\kappa$. The most important feature of this estimate is that it is independent of the mesh size.
Subsequently, we show that the new configuration, or any configuration with the magnetization of end domains parallel to the applied field, is energetically unstable. Thus the energy falls, as in the Stoner-Wohlfarth scenario, to its minimum value.

Assume that the applied field is decreasing so that $m^0 \approx e_1$. Let Ω^h denote the first and last columns of Ω, the closure domains, and set

$$m = m^{(h)} = \begin{cases} \xi & \text{in } \Omega^h \\ e_1 & \text{in } \Omega \backslash \Omega^h \end{cases}, \quad |\xi| = 1. \tag{5.1}$$

We now write the energy

$$E(H,m) = E(H,e_1) + \frac{E(H,m) - E(H,e_1)}{|\Omega^h|} |\Omega^h|$$

and determine a *shadow* energy

$$E_s(H,m^{(h)}) = E(H,e_1) + \lim_{h \to 0} \{ \frac{E(H,m^{(h)}) - E(H,e_1)}{|\Omega^h|} \} |\Omega^h| \tag{5.2}$$

Set

$$\psi^{(h)}(H,\xi) = \frac{1}{|\Omega^h|} (E(H,m^{(h)}) - E(H,e_1)) \text{ and } \psi^{(o)}(H,\xi) = \lim_{h \to 0} \psi^{(h)}(H,\xi). \tag{5.3}$$

The convergence above is uniform in H and ξ as $h \to 0$. The shadow energy will be

$$E_s(H,\xi) = E(H,e_1) + |\Omega^h| \psi^{(o)}(H,\xi) \tag{5.4}$$

A technical feature of working in two dimensions is that solutions of the equation

$$\Delta u = \operatorname{div} f, \text{ with } f \in L^2(\mathbb{R}^2) \tag{5.5}$$

are not in $H^1(\mathbb{R}^2)$ since the function u need not be square integrable over the whole space. Of course, we never need u but only ∇u, which is square integrable over the whole space, so we introduce the space

$$V = \{u \in H^1_{loc}(\mathbb{R}^2): \nabla u \in L^2(\mathbb{R}^2)\}. \tag{5.6}$$

Solving (5.5) in V leads to a slight ambiguity, which will be ignored, since u need not be unique, although ∇u is.

Consider the quantity

$$E(H,m^{(h)}) - E(H,e_1) = \int_\Omega (\varphi(m^{(h)}) - \varphi(e_1) - (m^{(h)} - e_1)\cdot H)\, dx$$

$$+ \frac{1}{2}\int_{\mathbf{R}^2} (|\nabla u^{(h)}|^2 - |\nabla w|^2)\, dx, \qquad (5.7)$$

where

$$w \in V: \Delta w = \frac{\partial}{\partial x_1}\chi_\Omega \quad \text{and} \quad u^{(h)} \in V: \Delta u^{(h)} = \operatorname{div} m^{(h)}\chi_\Omega \ \text{ in } \mathbb{R}^2. \qquad (5.8)$$

Also introduce w_o by

$$w_o \in V: \Delta w_o = \chi_\Omega \ \text{ in } \mathbb{R}^2.$$

We express the difference of the field energies in (2.1) as an integral over Ω^h by writing

$$\int_{\mathbf{R}^2} (|\nabla u^{(h)}|^2 - |\nabla w|^2)\, dx = \int_{\mathbf{R}^2} \nabla(u^{(h)} + w)\cdot\nabla(u^{(h)} - w)\, dx$$

$$= \int_\Omega \nabla(u^{(h)} + w)\cdot(m^{(h)} - e_1)\, dx$$

$$= \int_{\Omega^h} \nabla(u^{(h)} + w)\cdot(\xi - e_1)\, dx \qquad (5.9)$$

In order to evaluate the integral in (5.9), we use some facts about w and $u^{(h)}$ which are discussed in the appendix. Now $u^{(h)}$ is the solution of

$$\Delta u^{(h)} = \operatorname{div} m^{(h)}\chi_\Omega$$

$$= \operatorname{div} e_1\chi_\Omega + \operatorname{div} (\xi - e_1)\chi_{\Omega^h}.$$

Introducing the functions

$$w_1^{(h)} \in V: \Delta w_1^{(h)} = \frac{\partial}{\partial x_1}\chi_{\Omega^h} \quad \text{and}$$

$$w_2^{(h)} \in V: \Delta w_2^{(h)} = \frac{\partial}{\partial x_2}\chi_{\Omega^h}, \qquad (5.10)$$

we may write

$$u^{(h)} = w + (\xi_1 - 1)w_1^{(h)} + \xi_2 w_2^{(h)},$$

$$u^{(h)} + w = 2w + (\xi_1 - 1)w_1^{(h)} + \xi_2 w_2^{(h)}, \text{ and}$$

$$\nabla(u^{(h)} + w)\cdot(\xi - e_1) = 2(\xi_1 - 1)\frac{\partial w}{\partial x_1} + (\xi_1 - 1)^2\frac{\partial w_1^{(h)}}{\partial x_1} + \xi_2^2\frac{\partial w_2^{(h)}}{\partial x_2}$$

$$+ 2\xi_2\frac{\partial w}{\partial x_2} + \xi_2(\xi_1 - 1)(\frac{\partial w_1^{(h)}}{\partial x_2} + \frac{\partial w_2^{(h)}}{\partial x_1}).$$

We rewrite this expression using (A.4). Before performing this reduction, note that, $w_o(x) = w_o(x_1, 1 - x_2)$. This also holds for w. Thus this symmetry property implies that

$$\int_{\Omega\cap\{x_1=a\}} \frac{\partial w}{\partial x_2} dx_2 = 0, \quad 0 < a < L. \tag{5.11}$$

The same is true for $w_1^{(h)}$. Hence

$$\nabla(w + u^{(h)})\cdot(e_1 - \xi) = 2(\xi_1 - 1)\frac{\partial w}{\partial x_1} + (\xi_1 - 1)(2\xi_1\frac{\partial w_1^{(h)}}{\partial x_1} - (1 + \xi_1)\chi_{\Omega^h}) + I, \tag{5.12}$$

where by (5.11),

$$\int_{\Omega^h} I\, dx = 0.$$

From (5.12) we have

$$\int_{R^2} (|\nabla u^{(h)}|^2 - |\nabla w|^2)\, dx = 2(\xi_1 - 1)\int_{\Omega^h}\frac{\partial w}{\partial x_1} dx + (\xi_1 - 1)\int_{\Omega^h}(2\xi_1\frac{\partial w_1^{(h)}}{\partial x_1} - (1 + \xi_1))\, dx. \tag{5.13}$$

From (5.2) and (5.13), we have that

$$\psi^{(h)}(H,\xi) = \varphi(\xi) - \varphi(e_1) - (\xi_1 - 1)H_1 +$$

$$(\xi_1 - 1)\fint_{\Omega^h}\frac{\partial w}{\partial x_1} dx + \frac{1}{2}(\xi_1 - 1)\fint_{\Omega^h}(2\xi_1\frac{\partial w_1^{(h)}}{\partial x_1} - (1 + \xi_1))\, dx. \tag{5.14}$$

To pass to the limit as $h \to 0$ in (5.14), we refer to the appendix to note that $\frac{\partial w}{\partial x_1}$ and $\frac{\partial w_1^{(h)}}{\partial x_1}$ may be represented in terms of certain subtended angles and are continuous in Ω^h, $h > 0$, from which it follows by (A.9) and (A.13) that

$$\lim_{h\to 0} \fint_{\Omega^h} \frac{\partial w}{\partial x_1}\, dx = \int_{\Gamma_1} \frac{\partial w}{\partial x_1}\, dx_2 = \frac{1}{2} + \frac{1}{2\pi}\int_0^1 \theta_2(z)\, dx_2 = \lambda, \text{ and} \quad (5.15)$$

$$\lim_{h\to 0} \fint_{\Omega^h} \frac{\partial w_1^{(h)}}{\partial x_1}\, dx = \int_{\Gamma_1} \frac{\partial w_1^{(o)}}{\partial x_1}\, dx_2 = 1, \quad (5.16)$$

where $\Gamma_1 = \{ x_1 = 0, 0 < x_2 < 1 \}$.

This gives that

$$\psi^{(o)}(H,\xi) = \varphi(\xi) - \varphi(e_1) + (\xi_1 - 1)(\lambda - H_1) + \frac{1}{2}(\xi_1 - 1)^2. \quad (5.17)$$

At this point it is convenient to introduce

$$f(t,\xi) = \varphi(\xi) - \varphi(e_1) + (\xi_1 - 1)t + \frac{1}{2}(\xi_1 - 1)^2, \quad (5.18)$$

so that $\psi^{(o)}(H,\xi) = f(\lambda - H_1,\xi)$.

Recall that if $g(\xi)$, $|\xi| = 1$, has a local minimum at ξ_o, then

$$\nabla g(\xi_o)\cdot\xi_o^{\perp} = 0, \quad \xi_o\cdot\xi_o^{\perp} = 0, \text{ and}$$

$$\nabla^2 g(\xi_o)\cdot\xi_o^{\perp}\otimes\xi_o^{\perp} - \nabla g(\xi_o)\cdot\xi_o \geq 0. \quad (5.19)$$

Hence $\xi = e_1$ is a stable minimum of (5.18) for

$$\varphi(\xi) = \kappa\xi_2^2 \text{ or } \varphi(\xi) = \kappa\,\xi_1^2\xi_2^2 \text{ if } t < 2\kappa, \quad (5.20)$$

where $\kappa > 0$. Moreover, $f(2\kappa,\xi)$ has its unique local minimum at $\xi = -e_1$.

Consider now the uniaxial or cubic anisotropy energy with x_1 - axis easy. We see that the precursor magnetization $m = e_1$ of the shadow system is stable for

$$H_1 > -H_{cr} \text{ where } H_{cr} = 2\kappa - \lambda, \quad (5.21)$$

$$\lambda = \lambda(L) = \int_{\Gamma_1} \frac{\partial w}{\partial x_1}\, dx_2$$

$$= \frac{1}{2} + \frac{1}{\pi}\left(\arctan\frac{1}{L} - \frac{L}{2}\log\left(1 + \left(\frac{1}{L}\right)^2\right)\right). \quad (5.22)$$

We refer to $\lambda = \lambda(L)$ as the "magic number" of $(0,L)\times(0,1)$.

At $H_1 = -H_{cr}$, the stable magnetization is given by

$$\mu = m^{(h)} = \begin{cases} -e_1 & \text{in } \Omega^h \\ e_1 & \text{in } \Omega \setminus \Omega^h \end{cases} .$$

6. Complete shadow energy The shadow energy for the system (2.1) represents an effort to account for the effect of the demagnetization energy in a more general region than a disc but sufficiently simple that it can be easily calculated. Consider the special case $\Omega = (0,L) \times (0,1)$ which we regard divided into square elements as described in §3. To assemble the shadow energy, we shall assume that the magnetization m is constant in each column. By reducing in this way the number of degrees of freedom, we are able to accumulate the effects of the oscillations in the system without knowing their detailed structure. The complete simulated system, described in §3, does not retain constant magentization in each column and, when the applied field is nearly critical, evolves in a rather complicated fashion. For example, the intermediate plateaus on the falling energy portrait have been associated with magnetization reversal of a final pair of (horizontal) rows. Nonetheless, these events are confined to a very short interval of values of H and the general nature of the curve is characterized satisfactorily by our shadow energy.

Divide $\Omega = (0,L) \times (0,1)$ into N columns D_j separated by vertical segments T_j,

$$T_j = \{ \operatorname{Re} z = a_j \}, \quad a_j = jh, \; j = 0, \ldots, N, \tag{6.1}$$

with

$$D_j = \{ a_{j-1} < \operatorname{Re} z < a_j \} \cap \Omega, \quad j = 1, \ldots, N. \tag{6.2}$$

Consider magnetizations of the form

$$m = \sum_1^N \xi^j \chi_{D_j}, \quad |\xi^j| = 1. \tag{6.3}$$

Let

$$u \in V: \quad \Delta u = \operatorname{div} m. \tag{6.4}$$

The exact induced field energy is given by

$$\tfrac{1}{2} \int_\Omega \nabla u \cdot m \, dx = \tfrac{1}{2} \sum \int_{D_j} \nabla u \cdot \xi^j \, dx . \tag{6.5}$$

To approximate (6.5), begin with the introduction of the 2N functions v_k^j by

$$v_k^j \in V: \quad \Delta v_k^j = \frac{\partial}{\partial x_k} \chi_{D_j}, \; k = 1,2, \; j = 1,\ldots,N. \tag{6.6}$$

We may write

$$u = \sum \xi_k^j \, v_k^j \tag{6.7}$$

and

$$\frac{1}{2}\int_{\Omega}\nabla u\cdot m\,dx = \frac{1}{2}\sum\int_{D_j}(\xi_1^j\xi_1^k\frac{\partial v_1^k}{\partial x_1}+\xi_2^j\xi_2^k\frac{\partial v_2^k}{\partial x_2})\,dx+\frac{1}{2}\sum\int_{D_j}(\xi_2^j\xi_1^k\frac{\partial v_1^k}{\partial x_2}+\xi_1^j\xi_2^k\frac{\partial v_2^k}{\partial x_1})\,dx \tag{6.8}$$

Note that (v_1^j, v_2^j) satisfy the conditions (A.4). Using this and symmetry considerations, the second integral is seen to vanish and we may write (6.8) in the form

$$\frac{1}{2}\int_{\Omega}\nabla u\cdot m\,dx = \frac{1}{2}\sum_{j\neq k}(\xi_1^j\xi_1^k-\xi_2^j\xi_2^k)\int_{D_j}\frac{\partial v_1^k}{\partial x_1}dx$$

$$+\frac{1}{2}\sum_j((\xi_1^j)^2\int_{D_j}\frac{\partial v_1^j}{\partial x_1}dx+(\xi_2^j)^2\int_{D_j}\frac{\partial v_2^j}{\partial x_2}dx) \tag{6.9}$$

We shall approximate the integrals over the D_j by integrals on the vertical segments T_k. We use the approximations

$$\int_{D_j}\frac{\partial v_1^k}{\partial x_1}dx \approx h\int_{T_j}\frac{\partial v_1^k}{\partial x_1}dx_2 = -h\,a_{jk} \quad \text{for} \quad k > j,$$

$$\int_{D_j}\frac{\partial v_1^k}{\partial x_1}dx \approx h\int_{T_{j-1}}\frac{\partial v_1^k}{\partial x_1}dx_2 = -h\,a_{jk} \quad \text{for} \quad k < j, \tag{6.10}$$

with the convention that $a_{jj} = 0$. It is easily verified that $a_{jk} = a_{kj} > 0$. For $j = k$, we resort to our usual limiting process. Let $\theta^k(z)$ denote the angle subtended by T_k and z. Then, cf. A.9,

$$\frac{\partial v_1^j}{\partial x_1}(z) = \frac{1}{2\pi}(\theta^j(z)+\theta^{j-1}(z)), \quad z\in D_j,$$

$$\int_{D_j}\frac{\partial v_1^j}{\partial x_1}dx \approx h\int_{T_j}\frac{\partial v_1^j}{\partial x_1}dx_2\ , \text{and}$$

$$\int_{T_j}\frac{\partial v_1^j}{\partial x_1}dx_2 = \int_{T_j}\frac{1}{2\pi}(\pi+\theta^{j-1}(z))\,dx_2 = 1+O(h) \quad \text{as} \quad h\to 0.$$

Similarly,

$$\int_{D_j}\frac{\partial v_2^j}{\partial x_2}dx = O(h^2) \quad \text{as} \quad h\to 0.$$

We shall neglect the $O(h)$ terms in these coefficients. For $k > j$, note that

$$\frac{\partial v_1^k}{\partial x_1}(z) = \frac{1}{2\pi}(\theta^k(z) - \theta^{k-1}(z)),$$

$$a_{jk} = -\int_{T_j} \frac{\partial v_1^k}{\partial x_1} dx_2 = \int_{T_j} \frac{1}{2\pi}(\theta^{k-1}(z) - \theta^k(z))\, dx_2.$$

Now $a_{jk} = O(h)$, but we do not discard it since these terms are summed at various places. In fact, note that

$$f(a_k - a) = \frac{1}{2\pi} \int_{\mathrm{Re}\, z = a} \theta^k(z)\, dx_2 = \frac{1}{\pi}\int_0^1 \arctan\frac{t}{a_k - a}\, dt, \quad a < a_k.$$

For $a = a_j$, $a_k - a_j = h(k-j)$ and thus

$$a_{jk} = f((k-j-1)h) - f((k-j)h), \quad f(\sigma) = \frac{1}{\pi}\int_0^1 \arctan\frac{t}{\sigma}\, dt.$$

Identical considerations lead to the same formula for a_{jk} when $j > k$.

Using these approximations, we obtain a shadow approximation version of the induced field energy

$$\frac{1}{2}h\sum(\xi_1^j)^2 + \frac{1}{2}h\sum_{j\neq k} a_{jk}(\xi_2^j\xi_2^k - \xi_1^j\xi_1^k) \qquad (6.15)$$

with the a_{jk} defined by (6.10). The complete shadow energy is

$$E_s(H,\xi) = h\sum_j(\varphi(\xi^j) + \frac{1}{2}(\xi_1^j)^2 - \xi_1^j H_1) + \frac{1}{2}h\sum_{j\neq k} a_{jk}(\xi_2^j\xi_2^k - \xi_1^j\xi_1^k) \qquad (6.16)$$

This expression contains, of course, all the information of the preceding analysis, but is perhaps more difficult to manipulate, at least in the form given by (6.16). Let us use it to describe the easy axis picture.

Introduce the angles t_j by

$$\xi^j = (\cos t_j, \sin t_j), \quad 0 \le t_j \le 2\pi, \quad j = 1,\ldots,N, \text{ and}$$

$$g(t_j) = \varphi(\xi^j).$$

The shadow energy assumes the form

$$E_s(H,t) = h\sum_j (g(t_j) + \frac{1}{2}\cos^2 t_j - H_1\cos t_j) - \frac{1}{2}h\sum_{j\neq k} a_{jk}\cos(t_j + t_k) \qquad (6.17)$$

The equilibrium and stability conditions for a magnetization m of the form (6.3) are

$$\nabla_t E_s = 0 \quad \text{and} \quad \nabla_t^2 E_s \geq 0. \tag{6.18}$$

Note that

$$\frac{1}{h}\frac{\partial E_s}{\partial t_j} = g'(t_j) - \tfrac{1}{2}\sin 2t_j + H \sin t_j + \sum_k a_{jk} \sin(t_j + t_k), \tag{6.19}$$

$$\frac{1}{h}\frac{\partial^2 E_s}{\partial t_j^2} = g''(t_j) - \cos 2t_j + H \cos t_j + \sum_k a_{jk} \cos(t_j + t_k), \tag{6.20}$$

$$\frac{1}{h}\frac{\partial^2 E_s}{\partial t_j \partial t_k} = a_{jk} \cos(t_j + t_k), \; j \neq k. \tag{6.21}$$

Our tactic will be to solve (6.19) - (6.21) to within order h. For this reason we regard (6.21) as being satisfied. The stability condition of (6.18) then reduces to checking the definiteness of a diagonal matrix whose terms are given by (6.20). For ease of notation, we have replaced H_1 with H. Consider the case where

$$\varphi(\xi) = \kappa \xi_2^2 \quad \text{or} \quad g(\tau) = \kappa \sin^2\tau, \; \kappa > \tfrac{1}{2}. \tag{6.21}$$

corresponding to a uniaxial material with easy axis parallel to the side of the rectangle. Pertinent here is that $g'(0) = g'(\pi) = 0$ so that $m = e_1\chi_\Omega$ corresponding to $t_1 = t_2 = \ldots = t_N = 0$ is always an equilibrium as well as $m = -e_1\chi_\Omega$ or any combination of $t_j = 0$ or π. In these cases the critical field condition

$$\frac{1}{h}\frac{\partial E_s}{\partial t_j} = 0, \; j = 1, \ldots, N$$

is always satisfied. For large (positive) H, $m = e_1\chi_\Omega$ is a stable minimum. The condition (6.20) which governs its stability is

$$\frac{1}{h}\frac{\partial^2 E_s}{\partial t_j^2} = 2\kappa - 1 + H + \sum_k a_{jk} \geq 0, \quad j = 1, \ldots, N. \tag{6.20}$$

and we ask for the value of H where a mode becomes unstable, that is, where one of the terms above becomes negative.

The most systematic way to compute the sum in (6.20) is to return to the definition of the terms, which allows us to interpret it in terms of the magic numbers of subdomains of Ω. Now

$$\sum_k a_{jk} = \sum_{k=1}^{j-1} a_{jk} + \sum_{k=j+1}^{N} a_{jk}$$

$$= -\left\{ \sum_{k=1}^{j-1} \int_{T_{j-1}} \frac{\partial v_1^k}{\partial x_1} dx_2 + \sum_{k=j+1}^{N} \int_{T_j} \frac{\partial v_1^k}{\partial x_1} dx_2 \right\} + O(h).$$

Let w^j denote the solution of

$$\Delta w^j = \frac{\partial}{\partial x_1}\chi_{\Omega_{j-1}}, \quad \Omega_{j-1} = D_1 \cup \ldots \cup D_{j-1},$$

so that $w^j = \sum_{k=1}^{j-1} v_1^k$ and

$$\begin{aligned}\int_{T_{j-1}} \frac{\partial w^j}{\partial x_1} dx_2 &= \int_{T_{j-1}} \frac{1}{2\pi}(\theta^0(z) - \theta^{j-1}(z))\, dx_2 \\ &= \int_{T_{j-1}} \frac{1}{2\pi}(\theta^0(z) - \pi)\, dx_2 \\ &= \int_{T_{j-1}} \frac{1}{2\pi}(\theta^0(z) + \pi)\, dx_2 - 1 \\ &= \lambda((j-1)h) - 1 = \lambda(jh) - 1 + O(h),\end{aligned}$$

where $\lambda(s)$ is the magic number of $(0,s)\times(0,1)$. Thus

$$\sum_{k=1}^{j-1} a_{jk} = 1 - \lambda(jh) + O(h).$$

Similarly,

$$\sum_{k=j+1}^{N} a_{jk} = 1 - \lambda(L - jh) + O(h), \text{ and}$$

$$\sum_k a_{jk} = (1 - \lambda(jh)) + (1 - \lambda(L - jh)) + O(h).$$

In particular, note that $\lambda(0) = 1$ so

$$\sum_k a_{1k} = \sum_k a_{Nk} = 1 - \lambda(L) + O(h).$$

This gives that

$$\frac{1}{h}\frac{\partial^2 E_s}{\partial t_j^2} = 2\kappa - \lambda(L) + H + O(h), \qquad j = 1 \text{ and } j = N, \tag{6.21}$$

$$\frac{1}{h}\frac{\partial^2 E_s}{\partial t_j^2} = 2\kappa + 1 + H - (\lambda(jh) + \lambda(L - jh)) + O(h), \quad j = 2, \ldots, N-1. \tag{6.22}$$

We now claim that

$$\lambda(\sigma) + \lambda(L-\sigma) < \lambda(\sigma^*) + \lambda(L-\sigma^*) < \lambda(L) + 1 = \lambda(L) + \lambda(0), \quad 0 < \sigma^* < \sigma < \frac{L}{2}. \tag{6.23}$$

To check this recall that

$$\lambda(\sigma) = \tfrac{1}{2} + f(\sigma)$$

so that (6.23) reduces to checking that

$$f(\sigma) + f(L-\sigma) < f(\sigma^*) + f(L-\sigma^*) < f(L) + \tfrac{1}{2} = f(L) + f(0), \quad 0<\sigma^*<\sigma<\frac{L}{2}. \tag{6.24}$$

Now

$$f(\sigma) + f(L-\sigma) = \frac{1}{\pi}\int_0^1 (\arctan\frac{t}{\sigma} + \arctan\frac{t}{L-\sigma})\, dt$$

and

$$\frac{\partial}{\partial\sigma}(\arctan\frac{t}{\sigma} + \arctan\frac{t}{L-\sigma}) = (\frac{-1}{\sigma^2+t^2} + \frac{1}{(L-\sigma)^2+t^2})t < 0 \quad \text{for } 0<\sigma<\frac{L}{2}.$$

Thus (6.24) holds. Hence, $\frac{\partial^2 E_s}{\partial t_j^2} = \frac{\partial^2 E_s}{\partial t_{N-j}^2}$, $j \le [N/2]$, and

$$\frac{\partial^2 E_s}{\partial t_1^2} < \frac{\partial^2 E_s}{\partial t_2^2} < \ldots < \frac{\partial^2 E_s}{\partial t_{[N/2]}^2}. \tag{6.26}$$

The first modes to become unstable are $j = 1$ and $j = N$ and solving $\frac{\partial^2 E_s}{\partial t_1^2} = 0$ yields that

$$H = -H_{cr} + O(h) = -2\kappa + \lambda(L) + O(h), \tag{6.27}$$

in agreement with our prior result.

At H_{cr}, the new configuration obtained by variation of the unstable 1st and Nth modes is given by $t_1 = t_N = \pi$ and $t_2 = \ldots = t_{N-1} = 0$. From (6.20), we obtain the stability condition

$$\frac{1}{h}\frac{\partial^2 E_s}{\partial t_j^2} = 2\kappa - 1 - H_{cr} - \sum_k a_{jk} + 2a_{1N}, \qquad j = 1,N \tag{6.28}$$

$$\frac{1}{h}\frac{\partial^2 E_s}{\partial t_j^2} = 2\kappa - 1 + H_{cr} + \sum_k a_{2k} - 2(a_{12} + a_{2N}), \; j = 2, N-2, \tag{6.29}$$

with similar expressions for $2 < j < N-2$. We claim that (6.29) is negative at H_{cr}, and thus the columns the closure domain are rendered unstable by magnetization reversal in the closure domain. Repeating the argument we find that the stable configuration at $H = -H_{cr}$ is given by

$m = -e_1\chi_\Omega$, in other words, the system is unstable at $-H_{cr}$ and undergoes complete magnetization reversal.

We evaluate (6.29) for $j = 2$ which gives that

$$\frac{1}{h}\frac{\partial^2 E_s}{\partial t_2^2} = \lambda(L) + 1 - (\lambda(2h) + \lambda(L-2h)) - 2(a_{12} + a_{2N})$$

$$= \tfrac{1}{2} + f(L) + 1 - (\tfrac{1}{2} + f(2h) + \tfrac{1}{2} + f(L-2h)) - 2(\tfrac{1}{2} - f(h)) + O(h)$$

$$= -\tfrac{1}{2} + f(h) + O(h) < 0,$$

since f is decreasing and $f(0) = \frac{1}{2}$.

As we mentioned above, the configuration given by $t_1 = t_2 = t_{N-1} = t_N = \pi$ and $t_3 = \ldots = t_{N-2} = 0$ is now unstable, and so forth.

Another situation easily amenable to the same analysis is when the applied field is varied along the hardest axis corresponding to the present geometry with

$$\varphi(\xi) = \kappa(\xi_1)^2.$$

In this case, the precursor field $m = e_1$ loses stability at $H = 2\kappa + \lambda$ and, in contrast to the easy axis situation, there is no critical event, but the magnetization slowly evolves until reversal is complete at $H = -(2\kappa + \lambda)$. Brief inspection shows that to satisfy (6.19) and (6.20) in this case,

$$\frac{1}{h}\frac{\partial E_s}{\partial t_j} = g'(t_j) - \tfrac{1}{2}\sin 2t_j + H\sin t_j + \sum_k a_{jk}\sin(t_j + t_k) = 0, \qquad (6.19)$$

with $g(\tau) = \kappa\cos^2\tau$, gives rise to the equation

$$\frac{1}{h}\frac{\partial E_s}{\partial t_j} = (-(2\kappa + 1)\cos t_j + H)\sin t_j + \sum_k a_{jk}\sin(t_j + t_k) = 0.$$

This is satisfied approximately by

$$\cos t_j = \frac{H}{2\kappa + \lambda} \quad \text{for } H \text{ near } 2\kappa + \lambda.$$

and moreover in this range, (6.20) is positive.

7. Comparison with computation The table below summarizes our computational results. The data for both cases were taken from computations on a 16×8 grid but these were identical to the results from a 32×16 grid. In the uniaxial case the predicted value is nearly identical to the computed one. Samples of graphical renderings of the computations appear in Figures 4 - 7. The

range of values of the anisotropy constant κ was chosen so the energy stored in a body of constant magnetization was comparable to the induced field energy. To calculate the predicted values of the critical field we used (5.23) for $L = 2$ which gives a value $\lambda \approx 0.6$ and

$$H_{cr} = 2\kappa - 0.6. \tag{7.1}$$

κ	H_{cr} (predicted)	uniaxial H_{cr} (computed)	cubic H_{cr} (computed)
1	1.4	1.6	1.3
1.2	1.8	1.8	1.7
1.4	2.2	2.3	2.1
1.6	2.6	2.6	2.3
1.8	3.0	3.0	2.6
2.0	3.4	3.4	3

Table 1. Tabulated comparison of predicted and computed critical fields

We suspect that the variation we see in the cubic case owes primarily to the inadequacy of $m_o = e_1$ to serve as a precursor magnetization. A better precursor magnetization in this case might be somewhat tilted from the x_1 - axis at the four corners of Ω. Inspection of E_s as a function of ξ for a range of values of H suggests that e_1 dwells in a more shallow well in the cubic case than in the uniaxial one.

Computations of (2.1) with field varying along a hard axis have also been attempted. Our preliminary results indicate that the computed and predicted applied fields at which the uniform magnetization loses stability are in good agreement. In particular, the computations confirm that the demagnetization energy acts to destabilize the precursor field, which is also the situation for the field varying along the easy axis.

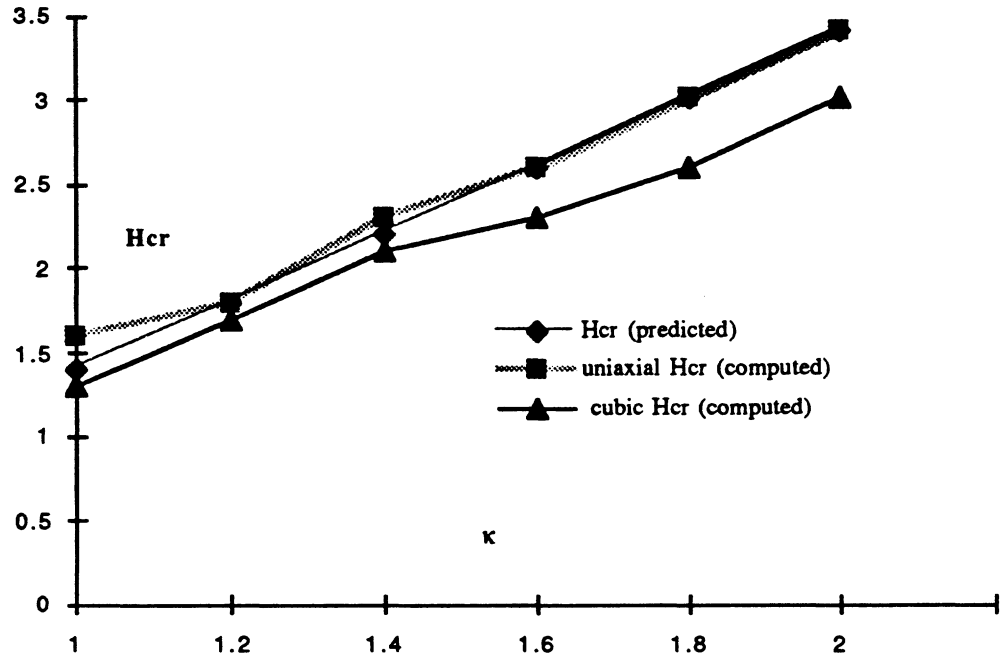

Figure 3. Comparison of predicted and computed critical fields

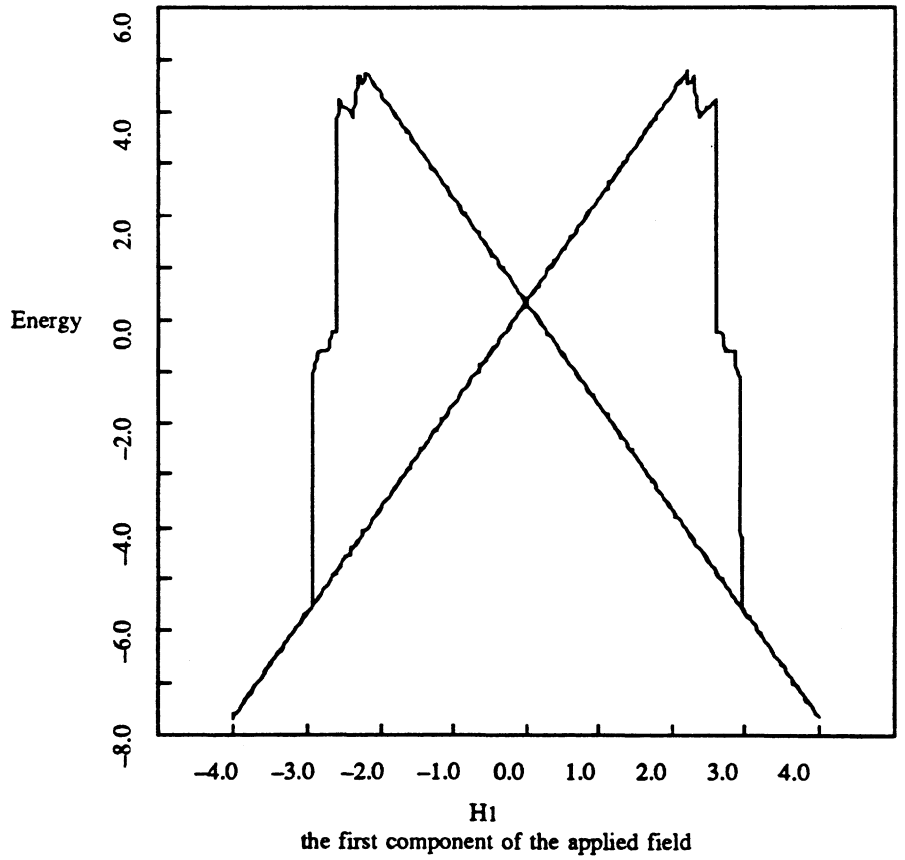

Figure 4. Computed hysteresis picture for uniaxial anisotropy energy (2.2) with $\kappa = 1.6$.

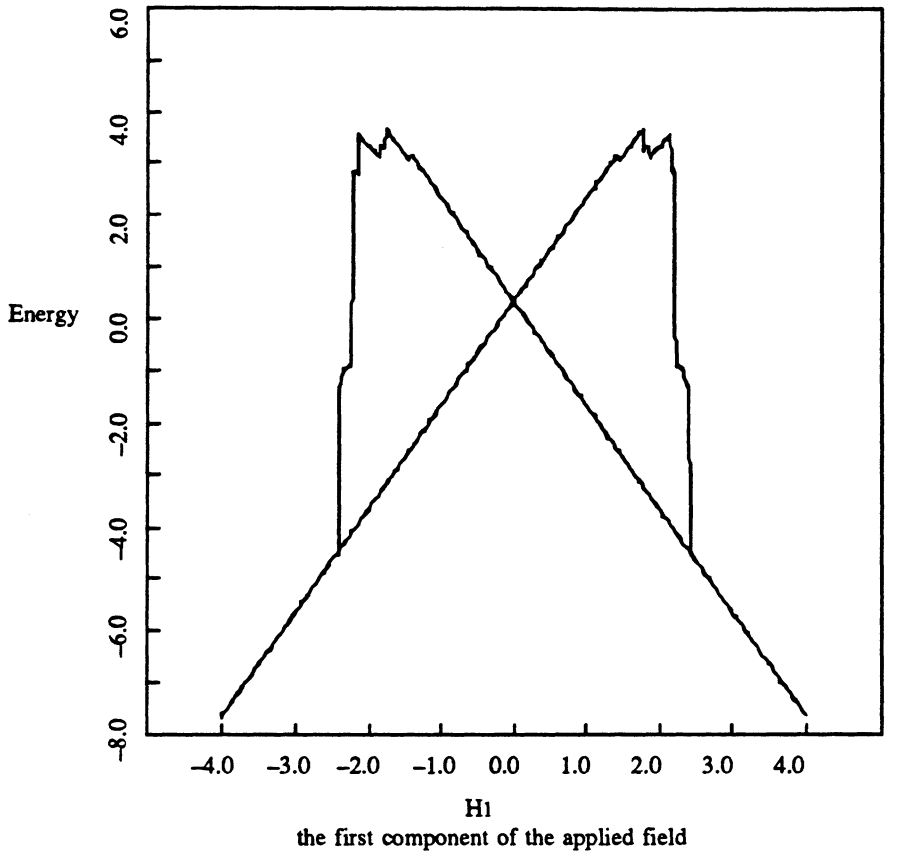

Figure 5. Computed hysteresis picture for cubic anisotropy energy (2.3) with $\kappa = 1.6$.

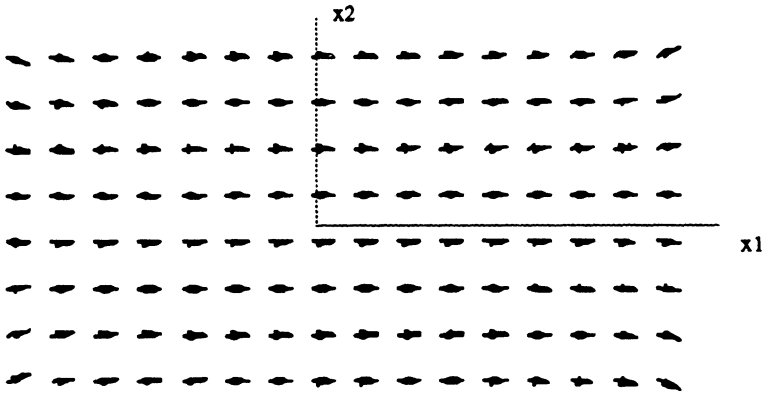

Figure 6. Computed magnetization configuration for uniaxial anisotropy energy (2.2) with $\kappa = 1.6$ at field value $H = (-2.1,0)$. This is in the metastable range.

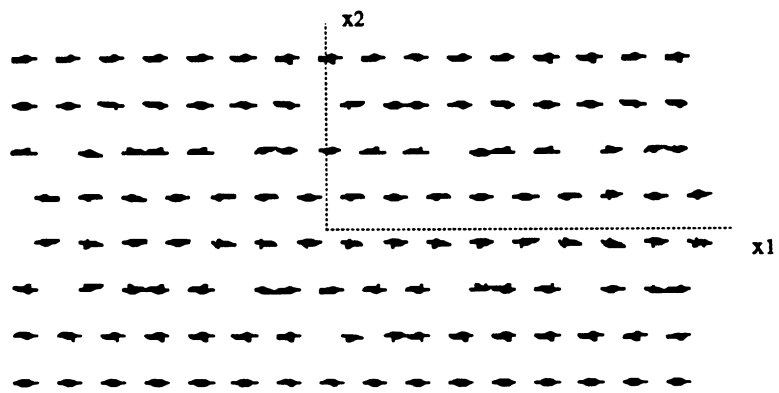

Figure 7. Computed magnetization configuration for uniaxial anisotropy energy (2.2) with $\kappa = 1.6$ at field value $H = (-2.32,0)$. This is in the unstable range.

8. Other systems Our conception is that most nonconvex computational optimization problems result in hysteretic behavior. As an example we have begun investigation of the Ericksen bar [13], which is a one dimensional version of a shape memory or pseudoelastic material. Hysteretic patterns of stress vs. load parameter in the extension of shape memory ribbons have been reported by Müller and Xu [35] and by Ortin [38], as cited earlier. Their observations, while quite different, share certain features, in particular the sequence of states passing from stable to metastable to unstable. These experiments, in which the orientation of the sample was not recorded, suggest attempting a simulation in one space dimension with an energy density which is not convex. This amounts to studying the well known Ericksen bar, which is also the topic of the analytic studies of Fedelich and Zanzotto [14] and Truskinovsky and Zanzotto [45]. The computation becomes a one dimensional version of (2.1), without, however, the induced field energy. We reproduced the general features of the experiments, but further investigation is necessary to understand if many details are also reproduced by our computations. Consideration of the shape memory ribbon as governed by a random hamiltonian has been studied by Sethna *et.al.* [42].

Appendix: a primer on solutions This section is an informal review of the properties of solutions of the equation

$$u \in V: \ \Delta u = \operatorname{div} \xi \chi_A, \ \text{with} \ \xi \in \mathbb{R}^2 \ \text{constant.} \qquad (A.1)$$

By combining the jump conditions implied for $\partial u/\partial \nu$ across ∂A with the Plemelj Formulas for Cauchy Integrals, cf. Muskhilishvili [36], an explicit representation for $\partial u/\partial z$ is easily derived. When $\xi = e_1$, say, and $A = \Omega$, Ω^h, or D^h, one of the rectangular regions which arise here, $\partial u/\partial x_1$ has a simple representation in terms of sums of angles subtended by certain vertical segments of ∂A.

Let A be a finitely connected region with piecewise smooth boundary ∂A and let u_o, u_1, and u_2 denote the solutions of

$$u_o \in V: \ \Delta u_o = \chi_A, \tag{A.2}$$

$$u_j \in V: \ \Delta u_j = \frac{\partial}{\partial x_j}\chi_A, \ j = 1,2, \tag{A.3}$$

where, as before,

$$V = \{u \in H^1_{loc}(\mathbb{R}^2): \nabla u \in L^2(\mathbb{R}^2)\},$$

which glosses over the fact that u itself need not be square integrable over the entire space since we are working in the plane. Equivalently,

$$u_j \in V: \ \int_{\mathbb{R}^2} \nabla u_j \cdot \nabla \zeta \, dx = \int_{\mathbb{R}^2} \chi_A \frac{\partial \zeta}{\partial x_j} dx, \ \zeta \in V, \ j = 1,2. \tag{A.3'}$$

It is easy to check that $u_j = \frac{\partial u_o}{\partial x_j}$, $j = 1,2$. Standard regularity theory applied to (A.3), or noting that $u_o \in H^{2,p}_{loc}(\mathbb{R}^2)$, shows that $u \in H^{1,p}_{loc}(\mathbb{R}^2)$, $1 \le p < \infty$. We note that

$$\operatorname{div}(u_1,u_2) = \chi_A \quad \text{and} \quad \operatorname{curl}(u_1,u_2) = 0 \quad \text{in } \mathbb{R}^2. \tag{A.4}$$

Moreover,

$$\frac{\partial u_j}{\partial z} = \frac{\partial u_j}{\partial x_1} - i\frac{\partial u_j}{\partial x_2}$$

is holomorphic in $\mathbb{R}^2 \backslash \partial A$. Hence we may represent $\frac{\partial u_j}{\partial z}$ as a Cauchy integral on ∂A with respect to an appropriate density. (A.3) and the piecewise smooth property of ∂A imply that

$$\frac{\partial u_j^+}{\partial \nu} - \frac{\partial u_j^-}{\partial \nu} = \nu_j$$

$$\frac{\partial u_j^+}{\partial \tau} - \frac{\partial u_j^-}{\partial \tau} = 0,$$

ν = outward pointing normal, τ = tangent

where $^+$ denotes the limit taken on approach from inside A and $^-$ denotes the limit taken on approach from $\mathbb{R}^2 \backslash A$.

For any function u,

$$\begin{pmatrix} \frac{\partial u}{\partial \tau} \\ \frac{\partial u}{\partial \nu} \end{pmatrix} = \begin{pmatrix} \nu_2 & -\nu_1 \\ \nu_1 & \nu_2 \end{pmatrix} \nabla u \quad \text{or} \quad \nabla u = \begin{pmatrix} \nu_2 & \nu_1 \\ -\nu_1 & \nu_2 \end{pmatrix} \begin{pmatrix} \frac{\partial u}{\partial \tau} \\ \frac{\partial u}{\partial \nu} \end{pmatrix}.$$

Hence

$$\frac{\partial u}{\partial z} = (\nu_2 + i\nu_1)\frac{\partial u}{\partial \tau} + (\nu_1 - i\nu_2)\frac{\partial u}{\partial \nu}. \tag{A.5}$$

Thus

$$\frac{\partial u_j^+}{\partial z} - \frac{\partial u_j^-}{\partial z} = (\nu_1 - i\nu_2)\nu_j \quad \text{on } \partial A, \qquad j = 1,2, \tag{A.6}$$

and according to the Plemelj Formula

$$\frac{\partial u_j}{\partial z}(z) = \frac{1}{2\pi i}\int_{\partial A}\frac{1}{t-z}(\nu_1 - i\nu_2)\nu_j\, dt\,, \; j = 1,2. \tag{A.7}$$

Now suppose that A is a rectangle with boundary consisting of segments parallel to the coordinate axes. Indeed, suppose that

$$\partial A = T_1 \cup T_2 \cup C, \text{ where}$$

$$T_j = \{ z \in \partial A: x_1 = a_j \}, \text{ with } a_1 < a_2,$$

and C consists of the segments parallel to the x_2 axis. Then $\nu_1 = 0$ on C and

$$\frac{\partial u_1}{\partial z}(z) = \frac{1}{2\pi i}\int_{T_1}\frac{1}{t-z}dt + \frac{1}{2\pi i}\int_{T_2}\frac{1}{t-z}dt\,, \; z \notin T_1 \cup T_2. \tag{A.8}$$

(If one does not write (A.8) as a contour integral, the sign of the first term is reversed.) The real parts of these integrals are merely the angles subtended by z and T_1 and T_2. For example, with $\theta_j(z)$ denoting the angle subtended by z and T_j,

$$\frac{\partial u_1}{\partial z}(z) = \frac{1}{2\pi}(\theta_1(z) + \theta_2(z)) - i\frac{\partial u_1}{\partial x_2}(z), \; z \in A.$$

Now $\theta_1(z) \to \pi$ as $z \to T_1$, giving that

$$\frac{\partial u_1^+}{\partial x_1}(z) = \frac{1}{2} + \frac{1}{2\pi}\theta_2(z), \; z \in T_1.$$

Similarly in view of (A.8),

$$\frac{\partial u_1}{\partial z}(z) = \frac{1}{2\pi}(\theta_1(z) - \theta_2(z)) - i\frac{\partial u_1}{\partial x_2}(z), \; \text{Re}\, z > a_2, \text{ and}$$

$$\frac{\partial u_1^-}{\partial x_1}(z) = -\frac{1}{2} + \frac{1}{2\pi}\theta_1(z), \; z \in T_2.$$

In general, we have the expression

$$\frac{\partial u_1}{\partial x_1}(z) = \begin{cases} \frac{1}{2\pi}(-\theta_1(z) + \theta_2(z)) & \text{Re } z < a_1 \\ \frac{1}{2\pi}(\theta_1(z) + \theta_2(z)) & a_1 < \text{Re } z < a_2 \\ \frac{1}{2\pi}(\theta_1(z) - \theta_2(z)) & \text{Re } z > a_2 \end{cases}, \qquad (A.9)$$

where $\theta_j(z)$ = the angle subtended by z and the segment T_j, $j = 1,2$.

We consider two special cases. Let $A = A_h = (0,h) \times (0,1)$ and consider $u_1^{(h)}$ with

$$u_1^{(h)} \in V: \ \Delta u_1^{(h)} = \frac{\partial}{\partial x_1} \chi_{A_h}.$$

Thus, with the obvious notations,

$$\frac{\partial u_1^{(h)}}{\partial z}(z) = \frac{1}{2\pi i} \int_{T_1} \frac{1}{t-z} dt + \frac{1}{2\pi i} \int_{T_{2,h}} \frac{1}{t-z} dt, \ z \notin T_1 \cup T_{2,h} \text{ and } (A.10)$$

$$\frac{\partial u_1^{(h)}}{\partial x_1}(z) = \frac{1}{2\pi}(\theta_1^{(h)}(z) + \theta_2^{(h)}(z)), \ z \in A_h. \qquad (A.11)$$

We further see that

$$\frac{\partial u_1^{(o)}}{\partial x_1}(z) = \lim_{h \to 0} \frac{\partial u_1^{(h)}}{\partial x_1}(z) = 1, \ z \in T_1 \text{ and}$$

$$\lim_{h \to 0} \fint_{A_h} \frac{\partial u_1^{(h)}}{\partial x_1}(z) \, dx_2 = 1 \qquad (A.12)$$

For the special case where $A = \Omega = (0,L) \times (0,1)$, retaining the notation $w = u_1$ employed in the body of the paper, and dropping the superscript $^+$,

$$\frac{\partial w}{\partial x_1}(z) = \frac{1}{2} + \frac{1}{2\pi}(\arctan \frac{t}{L} + \arctan \frac{1-t}{L}), \ z \in \Gamma_1, \ \text{Im } z = t, \text{ and} \qquad (A.13)$$

$$\int_{\Gamma_1} \frac{\partial w}{\partial x_1} dx_2 = \frac{1}{2} + \frac{1}{2\pi} \int_0^1 \theta_2(z) \, dx_2 = \lambda \qquad (A.14)$$

$$= \frac{1}{2} + \frac{1}{\pi}(\arctan \frac{1}{L} - \frac{L}{2} \log (1 + (\frac{1}{L})^2)).$$

Other situations may be calculated by superposition. For example, consider the region $A = \Omega^h$ or $A = D^h$. For definiteness, we take $A = \Omega^h$. Let $\Gamma_1^h = \{ x_1 = h, 0 < x_2 < 1 \}$

and $\Gamma_2^h = \{ x_1 = L - h, 0 < x_2 < 1\}$, and denote by $\theta_j^h(z)$ the angle subtended by Γ_j^h and z. Using (A.9) for each rectangle, we have for

$$w_1^{(h)} \in V: \ \Delta w_1^{(h)} = \frac{\partial}{\partial x_1} \chi_{\Omega h}.$$

that

$$\frac{\partial w_1^{(h)}}{\partial x_1}(z) = \frac{1}{2\pi}(\theta_1(z) + \theta_1^h(z) + \theta_2(z) - \theta_2^h(z)), \ 0 < x_1 < h, \text{ and} \quad (A.15)$$

$$\frac{\partial w_1^{(h)}}{\partial x_1}(z) = \frac{1}{2\pi}(\pi + \theta_1^h(z) + \theta_2(z) - \theta_2^h(z)), \ \mathrm{Re}\, z = 0, \text{ and}$$

$$\frac{\partial w_1^{(o)}}{\partial x_1}(z) = \lim_{h \to 0} \frac{\partial w_1^{(h)}}{\partial x_1}(z) = 1, \quad \mathrm{Re}\, z = L. \quad (A.16)$$

Acknowledgements

We wish to thank Antonio DeSimone, Richard James, Mitchell Luskin, Roy Nicolaides, and Noel Walkington for their help and advice in our investigations.

References

[1] Abeyaratne, R., Chu, C., and James, R. On the evolution of twinning microstructures in a CuAlNi shape memory alloy during biaxial dead loading (to appear)

[2] Ball, J. M.,Chu, C., and James, R. D. Metastability and hysteresis in elastic crystals (to appear)

[3] Berkov, D. V., *et al.* 1993 Solving micromagnetic problems, Phys. Stat. Sol., A137, 207-225

[4] Bruno, O., Leo, P., and Shields, T. 1993 Transient heat transfer effects on the pseudoelastic behavior of shape-memory wires, Acta Met. Mat., 5,191-201

[5] Chipot, M., Kinderlehrer, D., and Ma, L. to appear

[6] Clark, A. E. 1980 Magnetostrictive rare earth - Fe_2 compounds, *Ferromagnetic Materials, Vol 1* (Wohlfarth, E. P. ed) North Holland, 532 - 589

[7] Collins, C. and Luskin, M. 1989 The computation of the austenitic-martensitic phase transition, Lecture Notes in Physics 344 (ed. M. Rascle, D. Serre and M. Slemrod), Springer-Verlag, 34-50.

[8] Collins, C. and Luskin, M. 1991 Optimal order error estimates for the finite element approximation of the solution of a nonconvex variational problem, Math. Comp. 57, 621-637

[9] Collins, C., Kinderlehrer, D., and Luskin, M. 1991 Numerical approximation of the solution of a variational problem with a double well potential, SIAM J. Numer. Anal., 28, 321-333

[10] DeSimone, A. 1993 Energy minimizers for large ferromagnetic bodies, Arch. Rat. Mech. Anal., 125, 99-144

[11] DeSimone, A. 1994 Magnetization and magnetostriction curves from micromagnetics, J. Appl. Phys. 76, 7018-7020

[12] DeSimone, A. Hysteresis and imperfection sensitivity in small ferromagnetic particles (to appear)

[13] Ericksen, J. 1975 Equilibrium of bars, J. Elasticity, 5, 191-201

[14] Fedelich, B. and Zanzotto, G. 1992 Hysteresis in discrete systems of possibly interacting elements with a double well energy, J. Nonlinear Sci., 2, 319-342

[15] Giles, R., Alexopoulos, P. S., and Manuripur, M. 1992 Micromagnetics of thin film cobalt-based media for magnetic recording, Comp. in Physics, 6, 53-70

[16] Huo, Y., Müller, I., and Seelecke, S. 1994 Quasiplasticity and pseudoelasticity in shape memory alloys

[17] James, R. D. and Kinderlehrer, D. 1990 An example of frustration in a ferromagnetic material, Nematics: Mathematical and Physical Aspects, (Coron, J.-M., Ghidaglia, J.-M., and Hélein, F., eds), Kluwer NATO ASI series, 201-222

[18] James, R. D. and Kinderlehrer, D. 1990 Frustration in ferromagnetic materials, Cont. Mech. Therm., 2, 215-239

[19] James, R. D. and Kinderlehrer, D. 1992 Frustration and microstructure: an example in magnetostriction, *Prog Part Diff Eqns: calculus of variations, applications* (Bandle, C. et. al., eds) Pitman Res Notes Math 267, 59-81

[20] James, R. D. and Kinderlehrer, D. 1992 Twinned structures in terfenol, Proc. ICOMAT-92, Wayman, M. and Perkins, J., eds), 269-274

[21] James, R. D. and Kinderlehrer, D. 1993 A theory of magnetostriction with application to $TbDyFe_2$ Phil. Mag. B, 68, 237-274

[22] James, R. D. and Kinderlehrer, D. 1993 Mathematical approaches to the study of smart materials, *Mathematics in Smart Structures, Smart Structures and Materials '93*, Proceedings SPIE vol. 1919, (Banks, H. T., ed.) 2-18

[23] James, R. D. and Kinderlehrer, D. 1994 Theory of Magnetostriction with application to Terfenol-D, J. Appl. Phys., 76, 7012-7014

[24] Kinderlehrer, D., and Ma, L. 1994 Computational hysteresis in modeling magnetic systems, IEEE Trans. Mag., 30.6, 4380-4382

[25] Kinderlehrer, D., and Ma, L. 1994 Simulation of hysteresis in nonlinear systems, Math. and Control in Smart Structures, Proc. SPIE vol. 2192, (Banks, H.T., ed.),78-87

[26] Kinderlehrer, D., and Ma, L. The hysteretic event in the computation of magnetism and magnetostriction, Proc. Nonlinear Diff. Eqns. and their Appl., College de France Sem, Brezis, H. and Lions, J.-L., eds., (to appear)

[27] Kohn, R. 1991 The relaxation of a double-well energy, Cont. Mech. Therm., 3, 981-1000

[28] Luskin, M. and Ma, L. 1992 Analysis of the finite element approximation of microstructure in micromagnetics, SIAM J. Num Anal., 29, 320-331

[29] Luskin, M. and Ma, L. 1993 Numerical optimization of the micromagnetics energy, *Mathematics in Smart Structures, Smart Structures and Materials '93*, Proceedings SPIE vol. 1919, (Banks, H. T., ed.) 19-29

[30] Ma, L. 1993 Computation of magnetostrictive materials, *Mathematics in Smart Structures, Smart Structures and Materials '93*, Proceedings SPIE vol. 1919, (Banks, H. T., ed.) 47-54

[31] Ma, L. and Walkington, N. On algorithms for nonconvex optimization, to appear

[32] Macki, J. W., Nistri, P., and Zecca, P. 1993 Mathematical models for hysteresis, SIAM Review, 35, 94-123

[33] Mayergoyz, I. D. 1991 *The Preisach Model for Hysteresis*, Springer

[34] Müller, I. 1989 On the size of the hysteresis in pseucoelasticity, Cont. Mech. Therm., 1, 125-142

[35] Müller, I. and Xu, H. 1991 On the pseudoelastic hysteresis, Acta Metall., 39, 263-271

[36] Muskhelishvili, N. I. 1992 *Singular Integral Equations*, Dover (reprint of 1953 Noordhoff edition)

[37] Nicolaides, R. A. and Walkington, N. J. 1992 Computation of microstructure using Young measure representations, *Recent Advances in Adaptive and Sensory Materials and their Applications*, (Rogers, C. A. and Rogers, R. A., eds), Technomic, 1992

[38] Ortin, J. 1992 Preisach modeling of hysteresis for a pseudoelastic Cu-Zn-Al single crystal, J. Appl. Phys ,71,1454-1461

[39] Pedregal, P. 1994 Relaxation in ferromagnetism: the rigid case, J. Non. Sci.,4, 105-125

[40] Polak, E. 1971 *Computational methods in optimization* , Academic Press

[41] Rogers, R. C. 1991 A nonlocal model for the exchange energy in ferromagnetic materials, J. Int. Eqns. Appl., 3, 85-127

[42] Sethna, J., Dahmen, K., Kartha, S., Krumhansl, J., Roberts, B. and Shore, J. Hysteresis and heirachies: dynamics of disorder-driven first-order phase transitions, to appear

[43] Stoer, J. and Bulisch, R. 1993 *Introduction to numerical analysis, 2nd edition*, Springer

[44] Stoner, E. C. and Wohlfarth, E. P. 1948 A mechanisim of magnetic hysteresis in heterogeneous alloys, Phil. Trans. Royal Soc. (London) Sect A, 240, 599-642

[45] Truskinovsky, L. and Zanzotto, G. Eticksen's bar revisited (to appear)

[46] Visintin, A. 1994 *Differential models of hysteresis*, Springer

[47] Wiesen, K. and Charap, S. 1987 Vector Preisach modelling, J. Appl. Phys., 61, 4109-4021